

Experimental demonstration of Robust Amplitude Estimation on near-term quantum devices for chemistry applications

Alexander A. Kunitsa,^{1,*} Nicole Bellonzi,¹ Shangjie Guo,² Jérôme F. Gonthier,¹ Corneliu Buda,³ Clena M. Abuan,² and Jhonathan Romero¹

¹*Zapata Computing, Inc., 100 Federal St., Boston, MA 02110, USA*

²*Fuels & Low Carbon Tech - Digital Science, bp Technology,
501 Westlake Park Blvd, Houston, TX 77079, USA*

³*Technology LCP - Low Carbon Energy Advanced Bio & Physical Science,
30S Wacker Drive, Chicago, IL 60606, USA*

(Dated: October 2, 2024)

Abstract

This study explores hardware implementation of Robust Amplitude Estimation (RAE) on IBM quantum devices, demonstrating its application in quantum chemistry for one- and two-qubit Hamiltonian systems. Known for potentially offering quadratic speedups over traditional methods in estimating expectation values, RAE is evaluated under realistic noisy conditions. Our experiments provide detailed insights into the practical challenges associated with RAE. We achieved a significant reduction in sampling requirements compared to direct measurement techniques. In estimating the ground state energy of the hydrogen molecule, the RAE implementation demonstrated two orders of magnitude better accuracy for the two-qubit experiments and achieved chemical accuracy. These findings reveal its potential to enhance computational efficiencies in quantum chemistry applications despite the inherent limitations posed by hardware noise. We also found that its performance can be adversely impacted by coherent error and device stability and does not always correlate with the average gate error. These results underscore the importance of adapting quantum computational methods to hardware specifics to realize their full potential in practical scenarios.

I. INTRODUCTION

Continuous progress in quantum hardware brings us closer to demonstrating the utility of quantum computing for industrial applications. Quantum computing holds the promise of revolutionizing fields such as chemistry, materials science, and optimization by solving problems intractable for classical computers [1]. Since modern devices are limited in the qubit count, coherence times, and gate fidelities, the near-term quantum algorithms must be applied in tandem with error mitigation techniques or incorporate noise models in their design.

A prominent example of such algorithms is Robust Amplitude Estimation (RAE) [2, 3], an enhanced sampling technique that uses short-depth quantum amplitude amplification [4, 5] to accelerate observable estimation. It was initially developed to address the "measurement bottleneck" [6] plaguing variational algorithms, particularly the variational quantum eigensolver (VQE) [7]. To that end, RAE can reduce the scaling of the

* aakunitsa@gmail.com

number of state preparations needed to evaluate the VQE cost function with precision ϵ from $\mathcal{O}(\frac{1}{\epsilon^2})$ to $\mathcal{O}(\frac{1}{\epsilon^\alpha})$, where $\alpha \in [1, 2]$.

While RAE alone is likely not enough to make VQE practical [8], there are many cases where the estimation of expectation values is an essential component of a quantum algorithm that can benefit from RAE. Examples include estimating magnetization in quantum materials [9], simulation applications, the determination of properties over time-evolved solutions of differential equations [10, 11], or estimating Betti numbers in topological data analysis [12, 13]. This motivated further research into RAE-related algorithms, such as Quantum Amplitude Estimation (QAE) [4] and their applications outside the chemistry domain [14, 15].

The key feature of RAE is the ability to trade circuit depth to reduce the runtime. This flexibility comes at the cost of making the algorithm dependent on the device parameters, in particular, the gate fidelity [16]. Further, it assumes the depolarizing noise model accurately captures the underlying decoherence mechanisms. If this assumption is not satisfied in experiments on quantum hardware, special techniques, such as randomized compiling, need to be applied to ensure the validity of the RAE inference protocol. As shown by Dalal et al. [17], this is especially true in the presence of a coherent error severely limiting the scalability of RAE on near-term and possibly early fault-tolerant quantum devices. Therefore, it is critically important to assess the algorithm fitness for a particular application in a realistic setting.

Research has shown that early variants of QAE, such as Maximum Likelihood Quantum Amplitude Estimation (MLQAE) [4] and Iterative QAE (IQAE) [18], can offer practical advantages in NISQ environments by optimizing the balance between circuit depth and estimation accuracy [19]. These approaches help mitigate the errors introduced by quantum noise, allowing for more accurate results with fewer quantum resources. Furthermore, implementations of low-depth QAE algorithms on state-of-the-art quantum devices, such as trapped-ion quantum computers, have demonstrated significant improvements in accuracy when advanced techniques like the Chinese Remainder Theorem (CRT) and Maximum Likelihood Estimation (MLE) are employed [15]. These studies emphasize the need to tailor quantum algorithms to the specific noise characteristics and capabilities of the hardware to achieve optimal performance. In more recent research for reducing the quantum resources for observable estimation, Amplified Amplitude Esti-

mation (AAE) has emerged utilizing prior knowledge about the system to transform the problem into one where a small deviation from a known value can be efficiently estimated [20].

As most prior work on RAE and related techniques focused on optimizing circuit depth and mitigating noise in NISQ environments, the effects of these optimizations on the statistical properties of the estimation process have not been studied in detail, and the impact of specific quantum device characteristics such as noise profiles has been often overlooked. This may limit the practical applicability of these algorithms in real-world quantum computing tasks, where hardware imperfections are significant. In particular, it remains unclear how the convergence properties of RAE are affected by device parameter instability [21] and to what extent it can mitigate device noise when applied to estimating the expectation values of multi-term qubit operators, such as chemical Hamiltonians.

In this paper, we present an end-to-end implementation of RAE on a premium IBM device, *ibmq_montreal*, for estimating the ground state energy of one- and two-qubit Hamiltonians representing a model chemical system, H_2 . In contrast to the previous experimental demonstrations of RAE [16, 17], we focus on exploring the advantages and limitations of the algorithm from the classical Fisher information perspective drawing upon relevant methodological developments in QAE [5, 22]. We start by defining the estimation problem, reviewing the theory of RAE, and presenting the details of our hardware experiments and inference protocols in Sec. II. In Sec. III, we provide a context for choosing *ibmq_montreal* to demonstrate RAE and report the results of the one- and two-qubit RAE experiments followed by the analysis of factors impacting RAE performance. Finally, in Sec. IV, we summarize our findings and discuss future research directions.

II. TECHNICAL BACKGROUND

RAE is a technique that leverages low-depth quantum amplitude estimation to maximize information gain per measurement sample [2]. This is achieved by augmenting a state preparation circuit with a series of layers called Grover iterates. These layers enhance the sensitivity of measurement outcomes to the unknown expectation value compared to the standard sampling procedure of VQE. In a noiseless setting, this changes the scaling of estimation runtime with precision ϵ from $\mathcal{O}(1/\epsilon^2)$ (standard quantum limit) to

$\mathcal{O}(1/\epsilon)$ (Heisenberg limit), but in practice, the performance of the algorithm is curbed by noise and critically depends on how closely the noise profile of a realistic device resembles the exponential decay model.

A. H_2 Molecular Hamiltonians

In this study, we focus on the problem of estimating the ground state energy of the H_2 molecule, considering it in the STO-3G minimal basis. The ground state wave function of H_2 in this basis is a linear combination of two Slater determinants with doubly occupied σ_g and σ_u^* orbitals due to spin and symmetry constraints. To represent it on a quantum computer, one can either directly map it on a two-level problem encoded with one qubit or derive its two-qubit counterpart starting with a standard Jordan-Wigner mapping and performing qubit tapering [23].

In the first case, the Hamiltonian takes the form:

$$H = a^{(1)} + b^{(1)}X_0 + c^{(1)}Z_0, \quad (1)$$

where the parameters $a^{(1)}$, $b^{(1)}$, and $c^{(1)}$ were set to -0.329 , 0.181 , -0.788 , respectively. To estimate the ground state energy of the above Hamiltonian, we employ a single Y -rotation ansatz, optimized on a noiseless simulator:

$$|\Psi(\theta)\rangle = e^{-i\frac{\theta}{2}Y_0}|0\rangle, \quad (2)$$

with $\theta = -6.5095$. The expectation values of Pauli operators in Eq. 1 are $\langle X_0 \rangle = \sin(\theta) = -0.2243$ and $\langle Z_0 \rangle = \cos(\theta) = 0.9745$.

In the second case, we express the Hamiltonian as follows:

$$H = a^{(2)} + b^{(2)}Z_0 + c^{(2)}Z_1 + d^{(2)}Z_0Z_1 + e^{(2)}X_0X_1 + f^{(2)}Y_0Y_1, \quad (3)$$

with parameters $a^{(2)} = 0.2388$, $b^{(2)} = 0.3466$, $c^{(2)} = -0.4439$, $d^{(2)} = 0.5736$, $e^{(2)} = 0.09075$, and $f^{(2)} = 0.09075$. Following Ref. [23] and utilizing the Unitary Coupled-Cluster (UCC) ansatz [23, 24], we arrive at the following form of the ground state wave function¹:

$$|\Psi(\theta)\rangle = e^{-i\frac{\theta}{2}X_1Y_0}|01\rangle, \quad (4)$$

¹ It is assumed that the qubits are numbered from right to left, i.e. $|i_n, i_{n-1}, \dots, i_0\rangle$.

where θ is set to its optimal value -6.0575 . The expectation values of the Pauli strings in our two-qubit Hamiltonian (Eq. 3) can be evaluated analytically as functions of θ , resulting in $\langle Z_0 \rangle = -\cos(\theta) = -0.9746$, $\langle Z_1 \rangle = \cos(\theta) = 0.9746$, $\langle Z_0 Z_1 \rangle = 1$, and $\langle X_0 X_1 \rangle = \langle Y_0 Y_1 \rangle = -\sin(\theta) = -0.2238$.

B. RAE Ground State Energy Estimation

To estimate the ground state energy with RAE, one needs to evaluate the expectation values of individual unitary fragments of the corresponding Hamiltonian with respect to the ground state prepared by an ansatz circuit. Throughout this work, we used the most straightforward decomposition technique, in which unitary fragments are the Pauli strings. Each string requires a separate set of RAE circuits, even within the groups of commensurable operators [25–28].

A RAE circuit consists of an ansatz block A followed by a series of L Grover layers. The Grover layers are composed of a Pauli string P , whose expectation value needs measurement, and a reflection with respect to the state prepared by the circuit A , $R_A = 2|A\rangle\langle A| - \mathbb{I}$. The reflection operator is often represented using A and the "phase oracle" $R_0 = 2|0\rangle\langle 0| - \mathbb{I}$, $R_A = AR_0A^\dagger$, where R_0 acts as the identity operator on the state $|0\rangle$ and multiplies any orthogonal state by -1 ². The Grover layer sequence concludes with context selection gates chosen to rotate the final state to the eigenbasis of the Pauli string P . Examples of RAE circuits with one Grover layer are presented in Fig. 1.

More advanced methods, such as anti-commuting grouping [29], can boost RAE efficiency by reducing the number of expectation values to be evaluated. The corresponding RAE circuits will have the same structure as described above, with the Pauli operator P replaced by a more complicated unitary. The benefit of grouping can, therefore, be compromised by increased circuit depth. Exploring such trade-offs is beyond the scope of this work.

² Phase oracle can be implemented as a multi-controlled Z operation sandwiched between two layers of X gates. Depending on the device connectivity, it can be further compiled into a set of two-qubit gates, the number of which scales at least quadratically with the number of qubits [8].

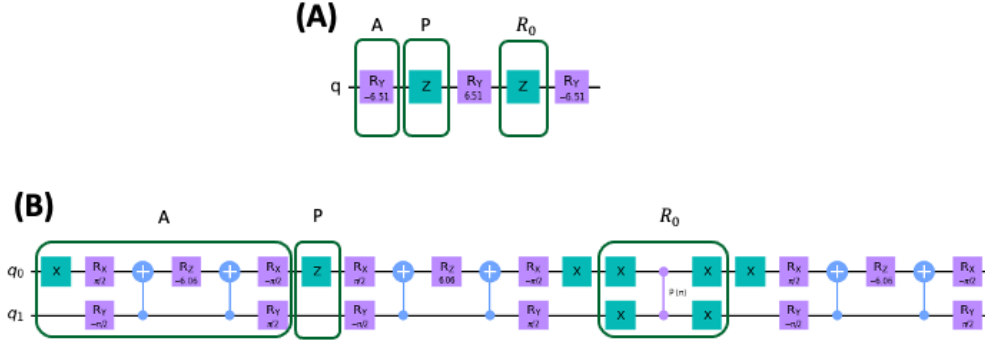


FIG. 1. Annotated RAE circuits with one Grover layer for estimating Z_0 operator for (A) one- and (B) two-qubit problems. Circuit elements (marked with A , P , and R_0) are defined in the main text.

C. Observable Estimation with Noise

Accurate estimation of observables from noisy quantum measurements is a fundamental task in quantum algorithms. Typically, in hardware implementations of VQE, measurements are performed on the qubit register in the standard basis (i.e., the basis of Pauli Z operators) to obtain the expectation values of individual Pauli strings Π_i or groups of co-measurable Pauli terms comprising an observable of interest $O = \sum_i c_i \Pi_i$ with respect to an ansatz state. In the simplest case, where a single Pauli string is considered, the measurement outcomes are modeled as Bernoulli random variables assuming values ± 1 with probabilities $p(\pm 1|\Pi) = \frac{1}{2}(1 \pm \Pi)$, where Π represents the unknown expectation value. After accumulating N samples, various approaches can be employed to estimate Π .

In what we will refer to as the *standard sampling*, the measurement outcomes are averaged to obtain an estimate of the unknown expectation $\hat{\Pi} = \frac{N_+ - N_-}{N}$, where N_{\pm} is the number of ± 1 among N measurement samples.

An alternative is to adopt a *Maximum Likelihood Estimation* (MLE) framework [30], wherein the unknown parameter is estimated by maximizing the total likelihood \mathcal{L} of the sample set defined as a product of the probabilities for individual samples:

$$\mathcal{L}(\mathbf{d}; \Pi) = \prod_{i=1}^N p(d_i|\Pi), \quad (5)$$

where $\mathbf{d} = (d_1, d_2, \dots, d_N)$ and $d_i = \pm 1$. In practice, however, it is more convenient to

maximize the log-likelihood defined as $l(\mathbf{d}; \Pi) = \log \mathcal{L}(\mathbf{d}; \Pi)$, yielding an estimate for Π , $\hat{\Pi} = \operatorname{argmax}_{\Pi} l(\mathbf{d}; \Pi)$.³ Substituting the expression for $p(\pm 1|\Pi)$ in Eq. 5 and finding the maximum of $l(\mathbf{d}; \Pi)$, it is straightforward to show that in this case, MLE is equivalent to the standard sampling. More generally, it can be applied to complicated estimation problems with multiple unknown parameters, and non-linear likelihood functions encountered in RAE, in which case Π is replaced with a vector $\mathbf{\Pi}$, and maximization needs to be carried out in a multi-dimensional space. Provided the estimate $\hat{\mathbf{\Pi}}$ is unbiased, the covariance matrix of the estimation error $\operatorname{cov}(\hat{\mathbf{\Pi}}) = \mathbb{E} [(\hat{\mathbf{\Pi}} - \mathbf{\Pi})(\hat{\mathbf{\Pi}} - \mathbf{\Pi})^T]$ ⁴ satisfies the Cramér-Rao (CR) bound

$$\operatorname{cov}(\hat{\mathbf{\Pi}}) \geq \mathcal{I}^{-1}(\mathbf{\Pi}), \quad (6)$$

where $\mathcal{I}(\mathbf{\Pi})$ is the Fisher information matrix with the matrix elements

$$[\mathcal{I}(\mathbf{\Pi})]_{i,j} = \mathbb{E} \left[\left(\frac{\partial}{\partial \Pi_i} \ln \mathcal{L}(\mathbf{d}; \mathbf{\Pi}) \right) \left(\frac{\partial}{\partial \Pi_j} \ln \mathcal{L}(\mathbf{d}; \mathbf{\Pi}) \right) \right].$$

If the CR bound is tight, the mean squared estimation error $\mathbb{E} [(\hat{\Pi} - \Pi)^2]$ is inversely proportional to Fisher information. Therefore, by maximizing information gain per sample, one can improve the efficiency of the estimation technique. In the context of RAE, this is achieved by modifying the likelihood function in a way that makes it more sensitive to the parameter of interest at the expense of increasing circuit depth. Under realistic experiment conditions, quantum circuits are subject to decoherence, limiting the maximum number of Grover iterates and the sampling boost offered by RAE. To describe noise effects on the estimation, we followed the standard approach adopted by Wang et al. [2] and assumed the global depolarizing noise under which an arbitrary n-qubit state ρ transforms into

$$\mathcal{E}_d(\rho) = p\rho + \frac{(1-p)}{2^n} \mathbb{I}, \quad (7)$$

where $p \in [0, 1]$ is the fidelity. If the action of the noise channel \mathcal{E}_d is interleaved with applying Grover iterates $U = R_A P$ (i.e. p is the Grover layer fidelity), an L -layer RAE circuit prepares a state

$$\rho_L = p^L U^L |A\rangle \langle A| (U^\dagger)^L + \frac{(1-p^L)}{2^n} \mathbb{I}. \quad (8)$$

³ $\operatorname{argmax}_y f(x; y)$ denotes the maximum value of f with respect to y for fixed x .

⁴ $\mathbb{E}(A)$ denotes the element-wise expectation value matrix of the matrix A , i.e. $\mathbb{E}(A)_{ij} = \mathbb{E}(A_{ij})$.

The first term in the above equation contains information about the observable of interest. Its amplitude decreases exponentially with L , following p^L . Although depolarizing noise may not accurately describe realistic quantum devices [17], it allows one to derive an analytic expression for the distribution of measurement outcomes, referred to as bitstring parities, from an L layer RAE circuit [2]:

$$\mathcal{P}_L(d|\Pi, \lambda) = \frac{1}{2} \left(1 + (-1)^d \text{Tr}[\rho_L P] \right) \quad (9)$$

$$= \frac{1}{2} \left(1 + (-1)^d e^{-\lambda(L+1/2)} T_{2L+1}(\Pi) \right), \quad (10)$$

In Eq. 10, Π is the expectation value of P with respect to the ansatz state, $\Pi = \langle A|P|A \rangle$, d is the bitstring parity ($d \in \{0, 1\}$), and $T_{2L+1}(\Pi) = \cos\{(2L+1) \arccos \Pi\}$ is the Chebyshev polynomial of the first kind. The effective noise parameter λ , is related to the Grover layer fidelity p , with $\lambda = -\ln(p)$. The exponent of the λ -dependent damping factor implies that the quantum state experiences twice as much decoherence from a single application of R_A as it does from the ansatz circuit A .

The likelihood function of RAE is a significant improvement over the one considered at the beginning of this section in several aspects. First, it explicitly incorporates noise via a single nuisance parameter λ . Second, it introduces an additional degree of freedom L to maximize Fisher information and reduce the MLE error. Non-linearity of $\mathcal{P}_L(d|\Pi, \lambda)$ gives rise to ambiguity in estimation since multiple values of Π can correspond to the same likelihood value. To ensure the uniqueness of the Π estimate, we combined MLE with a circuit fusion technique developed for low-depth QAE [4, 5] in which the total likelihood is computed as a product of the likelihood functions corresponding to varying Grover depth, L . The ordered set of L values, referred to as a "layer schedule", can be treated as a hyperparameter of the algorithm along with the number of measurement samples for each L [4, 5, 15, 31, 32]. The two commonly used layer schedules are "linearly incremental sequence" (LIS)

$$L_i = i, \quad (11)$$

and "exponentially incremental sequence" (EIS)

$$L_i = \lfloor 2^{i-1} \rfloor, \quad (12)$$

where $i = 0, 1, 2, \dots$. In a noiseless setting, if the number of samples is constant for different L_i , EIS results in the estimation runtime asymptotically approaching the Heisenberg

limit, i.e., scaling as $\mathcal{O}(1/\epsilon)$. By contrast, LIS corresponds to an intermediate regime between standard sampling and Heisenberg limit, $\mathcal{O}(1/\epsilon^{4/3})$. For a general polynomial schedule of degree d , i.e. $L_i = i^d$, the runtime scales as $\mathcal{O}(1/\epsilon^{(2d+2)/(2d+1)})$. As pointed out by Brown et al. [31], EIS yields a rapid increase in circuit depth and, as a result, tends to give a larger asymptotic error compared to LIS in the presence of noise. Away from the asymptotic regime EIS, however, can be superior to LIS. For this reason, we checked that LIS is equivalent to EIS in terms of the minimum estimation error for one of our experiments (Appendix D) and used the former throughout this work.

For any layer schedule \mathbf{L} under the assumption of N_s samples per circuit, the total likelihood takes the form:

$$\mathcal{L}(\mathbf{d}; \Pi, \lambda) = \prod_{L \in \mathbf{L}} \mathcal{P}_L(0|\Pi, \lambda)^{e_L} \mathcal{P}_L(1|\Pi, \lambda)^{N_s - e_L}. \quad (13)$$

Here, e_L denotes the number of even bit-strings observed for circuits with L layers. Using additivity of Fisher information with respect to the number of samples, one can derive the elements of the $\mathcal{I}(\Pi, \lambda)$ matrix corresponding to the likelihood function $\mathcal{L}(\mathbf{d}; \Pi, \lambda)$:

$$\mathcal{I}(\Pi, \lambda)_{11} = \sum_{L \in \mathbf{L}} \frac{N_s (2L + 1)^2 \sin^2((2L + 1) \operatorname{acos}(\Pi))}{(1 - \Pi^2) (e^{\lambda(2L+1)} - \cos^2((2L + 1) \operatorname{acos}(\Pi)))} \quad (14)$$

$$\mathcal{I}(\Pi, \lambda)_{12} = \sum_{L \in \mathbf{L}} \frac{N_s (L + 1/2)^2 \sin(2(2L + 1) \operatorname{acos}(\Pi))}{\sqrt{1 - \Pi^2} (-e^{\lambda(2L+1)} + \cos^2((2L + 1) \operatorname{acos}(\Pi)))} \quad (15)$$

$$\mathcal{I}(\Pi, \lambda)_{22} = \sum_{L \in \mathbf{L}} \frac{N_s (L + 1/2)^2 \cos^2((2L + 1) \operatorname{acos}(\Pi))}{e^{\lambda(2L+1)} - \cos^2((2L + 1) \operatorname{acos}(\Pi))} \quad (16)$$

Note that $\mathcal{I}(\Pi, \lambda)$ is singular if $\mathbf{L} = \{0\}$ for any λ and Π since the unknown parameters are not uniquely identifiable from MLE⁵. Adding extra measurements from the circuits with $L \neq 0$ removes the degeneracy, making $\mathcal{I}(\Pi, \lambda)$ invertible.

Assuming prior knowledge of λ and Π , one can use Eqs. 14-16 to compute the theoretical lower bound for the $MSE(\hat{\Pi})_{RAE}$ ⁶ according to the CR inequality. Similarly, it is straightforward to evaluate the MSE for the direct sampling estimator, establishing a reference for the RAE performance. In the presence of depolarizing noise, the ansatz circuit

⁵ This also follows from Eq. 10. Indeed, for $L = 0$, it can be shown that applying MLE results in an underdetermined system of equations.

⁶ In the following we use notation $MSE(\hat{\Pi})$ for the mean squared error of $\hat{\Pi}$, $\mathbb{E}[(\hat{\Pi} - \Pi)^2]$, with the subscript referring to the estimation method.

prepares the state

$$\rho_0 = e^{-\lambda/2}|A\rangle\langle A| + \frac{1 - e^{-\lambda/2}}{4}\mathbb{I}. \quad (17)$$

If one takes N_s measurements of the Pauli string P in state ρ_0 and averages the outcomes to estimate Π , the MSE of such estimator is

$$MSE(\hat{\Pi})_d = (1 - e^{-\lambda/2})^2\Pi^2 + \frac{1 - e^{-\lambda}\Pi^2}{N_s} \quad (18)$$

The CR bound combined with Eq. 18 yields a criterion to detect RAE sampling boost from experimental data. Specifically, we consider RAE to be successful in accelerating sampling on a real device whenever the empirical root mean squared error of the expectation of P , $RMSE(\hat{\Pi})$, is smaller than $\sqrt{MSE(\hat{\Pi})_d}$ for the *same number of ansatz queries*, i.e., the inequality

$$\sqrt{MSE(\hat{\Pi})_{RAE}} \leq RMSE(\hat{\Pi}) < \sqrt{MSE(\hat{\Pi})_d} \quad (19)$$

is satisfied with statistical accuracy. In practice, statistical error of the empirical $RMSE(\hat{\Pi})$ can either be estimated from a series of independent experiments or by performing bootstrapping on a single set of experimental results.

When applying RAE to measuring the expectation of a multi-term operator $O = \sum_i c_i \Pi_i$, it is important to consider an optimal shot allocation for measuring the expectations of Pauli terms it is comprised of. Although a solution to this problem is well known for direct sampling, the equivalent assignment of the number of circuit repetitions per Pauli $N_s^{(i)}$ is generally not available for RAE since $RMSE(\hat{\Pi}_i)$ is not known analytically as a function $N_s^{(i)}$. Although it is possible to establish an approximate runtime model for the single Pauli term estimation [8] and use it for measurement analysis, we chose to apply the uniform shot allocation for both RAE and direct sampling when calculating ground state energy, i.e., $N_s^{(i)} = N_s$. A more detailed analysis of the measurement allocation is left for future work.

D. Details of the experiments and post-processing

To evaluate RAE performance, we conducted two series of hardware experiments. In the first one, meant to probe the validity of the depolarizing noise model, we estimated

the likelihood of getting even bitstrings when measuring X_0X_1 , $\mathcal{P}_L(0|\Pi, \lambda)$ for $L = 1 - 5$ and 10 uniformly spaced values $\Pi \in [0, 1]$. The RAE circuits were implemented on *ibmq_hanoi* (QV⁷ 64), *ibmq_sydney* (QV 32), *ibmq_toronto* (QV 32), and *ibmq_montreal* (QV 128) quantum devices available on IBM quantum cloud as of 2021. 8192 shots were requested in each experiment. A readout correction was applied using the same number of shots to evaluate the measurement filters [35] for the appropriate qubit subsets. To reconstruct $\mathcal{P}_L(0|\Pi, \lambda)$ from our experiments we estimated the expectation values of X_0X_1 with respect to ρ_L and applied Eq. 9. The error bounds were computed from empirical standard deviations of the X_0X_1 expectation values. Chebyshev likelihood functions (Eq. 10) were fitted to experimental data to extract effective noise parameters λ using `scipy.optimize.curve_fit` [36]. The standard error of λ , $\delta\lambda$, was computed as a square root of its variance estimated using a linear approximation to the model function near the optimum. In the second series of experiments, we estimated the ground state energies of the one- and two-qubit Hamiltonians (Eq. 1 and Eq. 3) on *ibmq_montreal* with RAE. Experiments involved submitting RAE circuits created individually for each term in corresponding Hamiltonians and terminated with the appropriate context selection gates. The maximum number of Grover iterates was set to 10 and 8 for one- and two-qubit circuits, respectively, with 8192 samples per circuit. As described in Sec. II C, the expectation values of the Pauli terms were extracted from experimental data via MLE. To determine the error bounds of the estimates, we applied *bootstrapping* [30, 37] following Refs. [16, 17]. Specifically, given a layer schedule \mathbf{L} , we generated a list of maximum likelihood estimates for each Pauli term P by resampling 8192 bitstring parities with repetitions from each $L \in \mathbf{L}$ and using them to compute and maximize the log-likelihood $l(\mathbf{d}; \Pi, \lambda)$. Given the list of M estimates $\{\hat{\Pi}_i\}_1^M$ we computed $MSE(\hat{\Pi})$ as

$$MSE(\hat{\Pi}) = \frac{1}{M} \sum_i (\Pi_i - \Pi)^2 \quad (20)$$

The empirical variance of $MSE(\hat{\Pi})$ was taken as a measure of its statistical error and was evaluated as

$$\mathbb{V}(MSE(\hat{\Pi})) = \frac{1}{M} \sum_i \{(\Pi_i - \Pi)^2 - MSE(\hat{\Pi})\}^2 \quad (21)$$

⁷ QV = Quantum Volume [33, 34]

Standard error propagation formula was applied to $\mathbb{V}(MSE(\hat{\Pi}))$ to obtain statistical error of $RMSE(\hat{\Pi}) = \sqrt{MSE(\hat{\Pi})}$:

$$\sigma = \frac{\sqrt{\mathbb{V}(MSE(\hat{\Pi}))}}{2 \cdot RMSE(\hat{\Pi})} \quad (22)$$

When post-processing the results of RAE experiments, we chose $M = 15000$ and $M = 10000$ for one-qubit and two-qubit circuits, respectively.

In all cases, the circuits were submitted via Qiskit [38] with the optimization level set to 0, which resulted in the transpiler expressing the circuits in the native gate set and mapping them to qubits 0 and 1.

III. RESULTS

The goal of our experiments was to probe several aspects of RAE, including (a) the impact of realistic hardware noise on the convergence of expectation values, (b) sampling rate increase compared to the standard approach, and (c) the error mitigation properties reported by Dalal et al. [17]. Below, we commented on the aforementioned aspects of RAE in the context of one- and two-qubit ground-state energy estimation problems considered in this work. As a prerequisite, we investigated the relevant properties of the quantum devices considered in this work and extracted the effective noise parameter λ from RAE data for *ibmq_montreal* in Sec. III A and Sec. III B. The values of λ were used as inputs to the direct sampling and RAE performance models discussed in Sec. III C.

A. Noisy likelihood functions and RAE performance

A preliminary assessment of the validity of depolarizing noise as a model for decoherence effects in our experiments can be made based on how well Eq. 10 describes empirical likelihood functions. We found that it captures their overall shapes with some discrepancies, the magnitude of which differs between the devices and can be quantified by the standard errors of the λ values extracted from non-linear fits. As one can see in Fig. 2 (Panel A), the depolarizing noise model is the least accurate for *ibmq_hanoi*, and its accuracy does not strongly correlate with the QV. Furthermore, the values of λ vary with the number of Grover iterates.

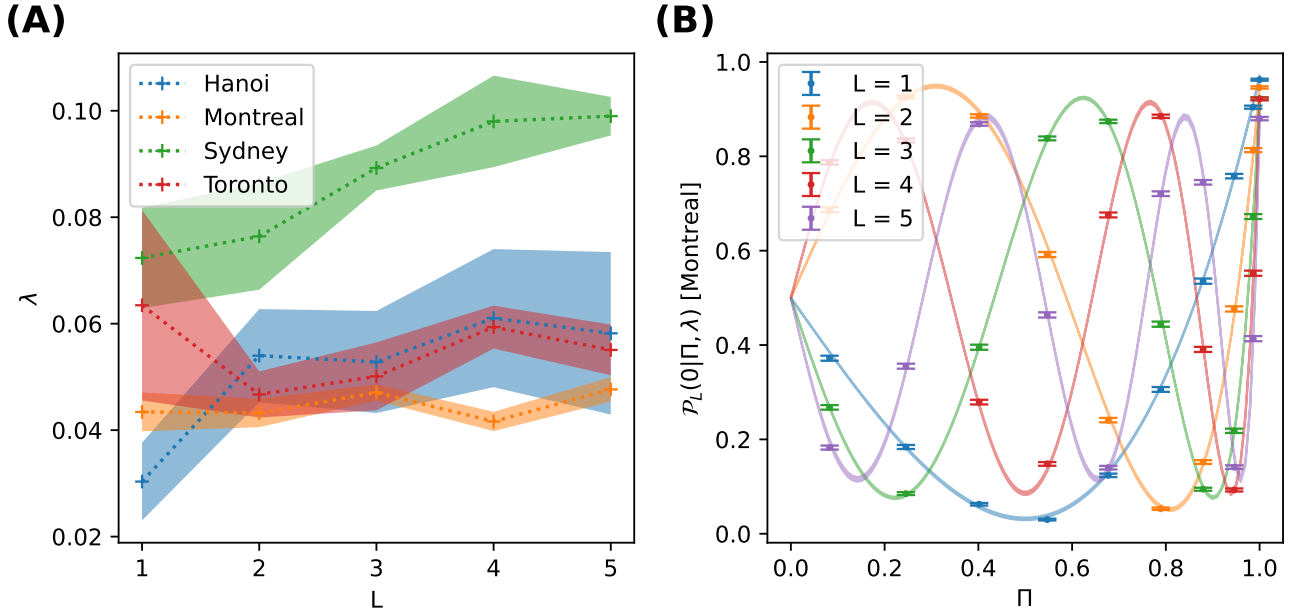


FIG. 2. (Panel (A): effective noise parameters λ as functions of the RAE circuit depth (the number of Grover iterates, L) on IBM quantum devices. Shaded areas correspond to $\lambda \pm \delta\lambda$ values obtained via non-linear fit. Panel (B): measured likelihood function (points with error bars) fitted to $\mathcal{P}_L(0|\Pi, \lambda)$ (solid lines) for $L = 1 - 5$ on *ibmq_montreal*. The numerical values of λ and their errors are presented in Tab. A1. Line width demonstrates the variation of the likelihood function with the noise parameter $\in [\lambda - \delta\lambda, \lambda + \delta\lambda]$

This behavior has not been previously observed in the context of RAE and is likely due to the device parameter instability reported by other authors in a more general benchmarking setting [21]. Since the RAE inference protocol assumes a noise parameter independent of L , we expect a noticeable impact on the algorithm performance due to the variation of λ . In principle, this restriction can be removed with a more flexible multi-parameter likelihood function [22] at the expense of more complicated post-processing and a different experimental setup relying on additional assumptions about the noise model.

Comparing the degree of λ variation between the devices considered in this work, we note that *ibmq_montreal* is the most stable (λ changes by at most 14%), while the performance of the other three QPUs is roughly similar (with λ varying by about 50% in some cases). Another favorable feature of *ibmq_montreal* is the close agreement between its like-

likelihood function and Eq. 10 as can be seen in Fig. 2 (Panel B) suggesting the validity of the depolarizing noise model for this device.

For these reasons, we chose *ibmq_montreal* to demonstrate RAE performance. In the following sections, we showed that the criterion in Eq. 19 was satisfied in most of the RAE experiments on that backend, indicating a sampling acceleration compared to the direct method commonly used in VQE. Furthermore, RAE demonstrated noise mitigation properties in some cases, allowing RMSE reduction for Z_0 and Z_1 Pauli terms in the two-qubit Hamiltonian by about one order of magnitude compared to the asymptotic direct sampling limit. The combined effect of sampling boost and noise mitigation resulted in ground state energy estimates within chemical accuracy for both one- and two-qubit problems. This contrasts with the results from direct sampling for the two-qubit problem and marks a significant improvement in accuracy for the one-qubit problem.

B. Effective noise parameters and direct sampling performance

To model direct sampling and RAE performance based on the theoretical CR bound, we extracted the effective noise parameters λ from RAE results via MLE (Fig. 3 and Fig. 4). For both one- and two-qubit cases, λ estimates converge with the Grover depth, L_{max} reaching asymptotic values that are close but not identical for different Pauli terms. This can be explained by the differences in RAE circuit transpilation. Further, the noise levels for the one-qubit circuits are about one order of magnitude lower than for the two-qubit case, in line with average one- and two-qubit gate fidelities.

MLE provides an independent way to validate the value of λ obtained as described in the previous section for X_0X_1 . In Fig. 4, one can see that the two methods provide consistent results within the error bounds.

In the following, we used MLE-derived λ values to model the performance of the direct sampling with the number of ansatz queries as prescribed by Eq. 18. Similarly, λ enters the CR bound for the RAE MSE. It is, therefore, crucial to ensure that the estimates of λ accurately represent the device performance. It can be shown that although RAE results for $L_{max} = 0$ are insufficient for simultaneous observable and noise estimation, using them as an input for MLE with $\lambda = 0$ is equivalent to the direct observable estimation. We relied on this property to derive reference expectation values for the Pauli

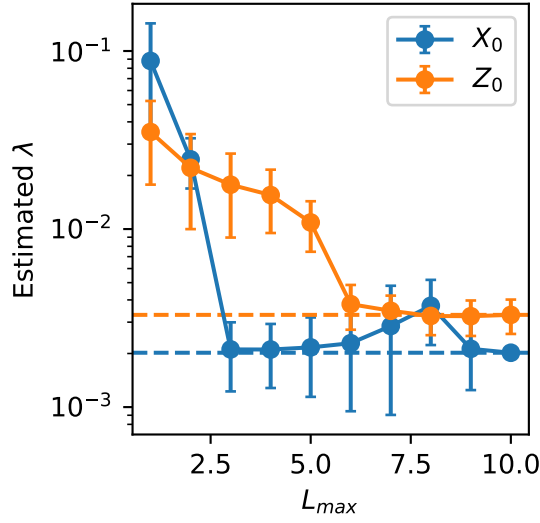


FIG. 3. Convergence of the λ values estimated via MLE for the Pauli terms in the one-qubit Hamiltonian (Eq. 1). The error bars were calculated as standard deviations of the bootstrapped $\hat{\lambda}$ values as explained in Sec. II D. L_{max} refers to the maximum Grover depth used to estimate λ . Dashed lines indicate the converged values of the noise parameter.

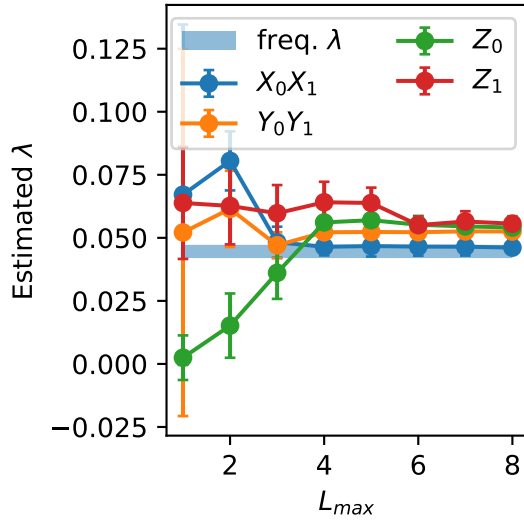


FIG. 4. Convergence of the λ values estimated via MLE for the Pauli terms in the two-qubit Hamiltonian (Eq. 3). L_{max} refers to the maximum Grover depth used in the estimation. The boundary of the filled area corresponds to $\lambda \pm \delta\lambda$, i.e., the range of noise parameter values determined by fitting the Chebyshev likelihood functions of X_0X_1 to the experimental estimates for $L_{max} = 1 - 5$.

Π	ϵ	ϵ (analytic)
<i>One-qubit Hamiltonian</i>		
$\langle Z_0 \rangle$	0.0045(0) ^{ab}	0.0030
$\langle X_0 \rangle$	0.0510(105)	0.0108
<i>Two-qubit Hamiltonian</i>		
$\langle Z_0 \rangle$	0.0083(28)	0.0262
$\langle Z_1 \rangle$	0.0246(3)	0.0270
$\langle Y_0 Y_1 \rangle$	0.0119(82)	0.0122
$\langle X_0 X_1 \rangle$	0.0200(99)	0.0119

^a statistical error is less than 10^{-4}

^b shorthand notation is used for the floating point numbers with finite statistical precision replacing $X.XXXX \pm 0.00YY$ with $X.XXXX(YY)$

TABLE I. Root mean square errors ϵ of the Pauli expectations computed from experimental data collected in one- and two-qubit RAE experiments and estimated analytically (based on (Eq. 18), i.e. $\epsilon = \sqrt{MSE(\hat{\Pi}_d)}$ assuming effective noise parameters from MLE.

terms in the corresponding Hamiltonians and perform additional consistency checks for the noise parameters. In Tab. I, we compared RMSE of the Pauli expectations extracted from RAE experiments with $L = 0$ with the predictions of Eq. 18 assuming λ values from MLE.

As can be seen from the table, there exist discrepancies between experimental ϵ and its analytical estimate from Eq. 18 that cannot be attributed to statistical errors (for example, for Z terms). In many cases where the two differ, however, the direct sampling model yields smaller RMSEs than the experiment, except for Z_0 and Z_1 terms in the two-qubit Hamiltonian. Effectively, this means that MLE underestimates the noise parameter for direct sampling, lowering the upper boundary of the RAE advantage window, as follows from the criterion in Eq. 19. For this reason, we used Eq. 18 with λ from MLE when assessing the RAE sampling boost despite the associated discrepancies with a caveat that it may not be reliably detected in the experiments where we measured Z_0 and Z_1 expectation values.

C. RAE application to ground state energy estimation

Having established the performance models for RAE and direct sampling, we analyzed our experiments from the perspective of the sampling advantage criterion Eq. 19.

Turning to the one-qubit case presented in Fig. 5, we observed qualitatively different behavior for X_0 and Z_0 . RMSE for the former is higher than the direct sampling values, while the latter benefits from RAE sampling acceleration. Partially, this might be due to low bias for X_0 , giving rise to a relatively small RMSE dominated by the variance. As a result, RMSE reduction gives rise to a very narrow advantage window for X_0 . The noisy CR bound is far from saturation in both cases and closely agrees with the noiseless one, showing no distinct plateau [5]. Based on the form of the likelihood function, one could expect ϵ to plateau at approximately $1/\lambda \approx 300 - 500$. Accumulation of coherent error at such high Grover depth would likely compromise RAE performance long before the limit is reached. The signs of this behavior can be seen in a non-monotonous decrease of the RAE estimation error for Z_0 .

Similar patterns persist for the two-qubit experiments where RAE outperforms direct sampling for the terms with high bias (Z_0 and Z_1) even at $L_{max} = 1$, while a larger Grover depth is required to observe advantage for the low-bias terms (X_0X_1 and Y_0Y_1). Although the sampling boost for Z_0 cannot be established reliably due to imperfections in the direct sampling performance model, one can still expect to observe the error reduction compared to direct sampling if $\epsilon = 10^{-3}$ is taken as a conservative estimate of the direct sampling error (Tab. I).

Comparing one- and two-qubit experiments, we observed that the noise levels did not correlate with the RAE efficiency as long as the underlying decoherence mechanism was consistent with the depolarizing noise assumption. In that case, RAE can effectively learn to eliminate noise as a part of the estimation process, as suggested by Ref. [17] and corroborated by our results. In the experiments for X_0X_1 and Y_0Y_1 , the minimum estimation error was achieved at the intermediate Grover depth, $L_{max} = 4$. This coincides with the value at which parameter instability developed in preliminary experiments on *ibmq_montreal* (Fig. 2), providing indirect evidence of RAE performance being sensitive to the fluctuation of λ .

To estimate the ground state energy with RAE, the expectation values of the individual

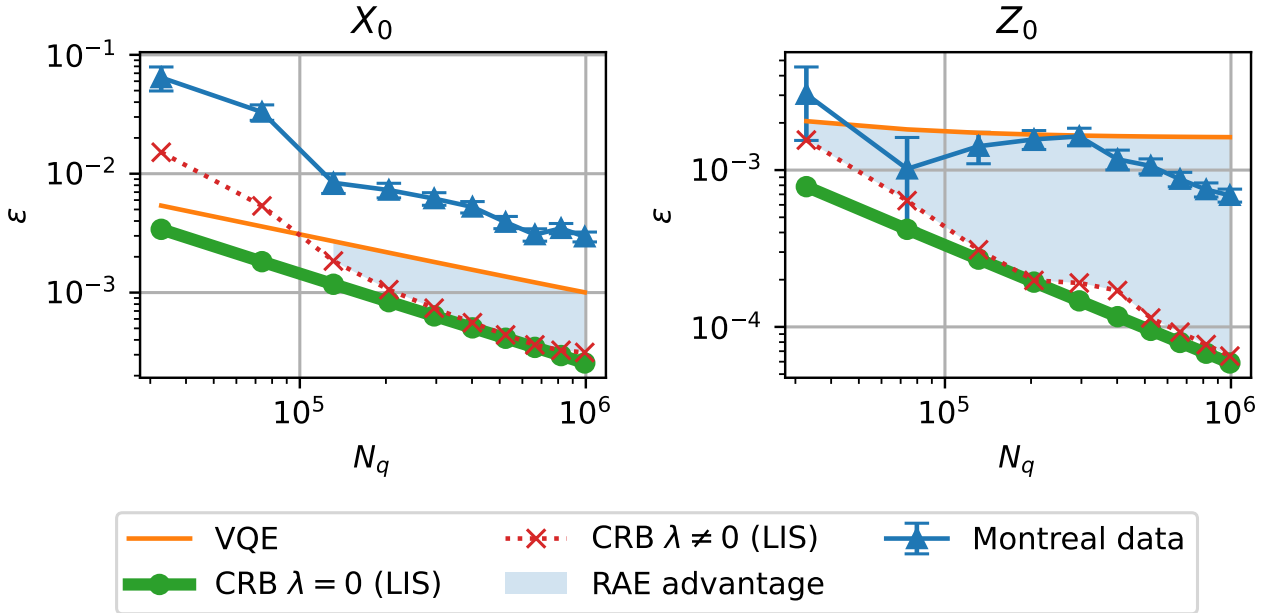


FIG. 5. RMSE of the estimated Pauli terms in the one-qubit Hamiltonian (Eq. 1). N_q refers to the total number of ansatz queries across all RAE circuits to obtain a Pauli term expectation. RMSE of the direct sampling estimator (marked VQE in the figure) was modeled based on the effective noise parameter extracted from RAE data. CRB refers to the lower estimate of RMSE based on the Cramer-Rao bound (Eq. 6).

Pauli terms were combined with appropriate weights. The variance of the estimator was computed using the standard expression for the linear combination of random variables. Energy bias and variance were then used to calculate RMSE presented in Fig. 7. A similar calculation was performed for the direct sampling using analytic expressions for the bias and variance under the assumption of depolarizing noise with λ parameters determined via MLE. In both cases, we assumed the uniform allocation of ansatz queries N_q across Pauli terms in corresponding one- and two-qubit Hamiltonians.

For the one-qubit Hamiltonian, despite the relatively large estimation error for the X_0 , the RMSE ground state energy falls below chemical accuracy for the one-qubit Hamiltonian when $L_{max} > 2$ since the term enters with a smaller coefficient compared to Z_0 . Although direct sampling reaches the chemical accuracy threshold sooner than RAE, the final RMSE for the latter is much lower, below 0.1 mH (Fig. 7).

The ground state energy RMSE for the two-qubit Hamiltonian exhibited a similar con-

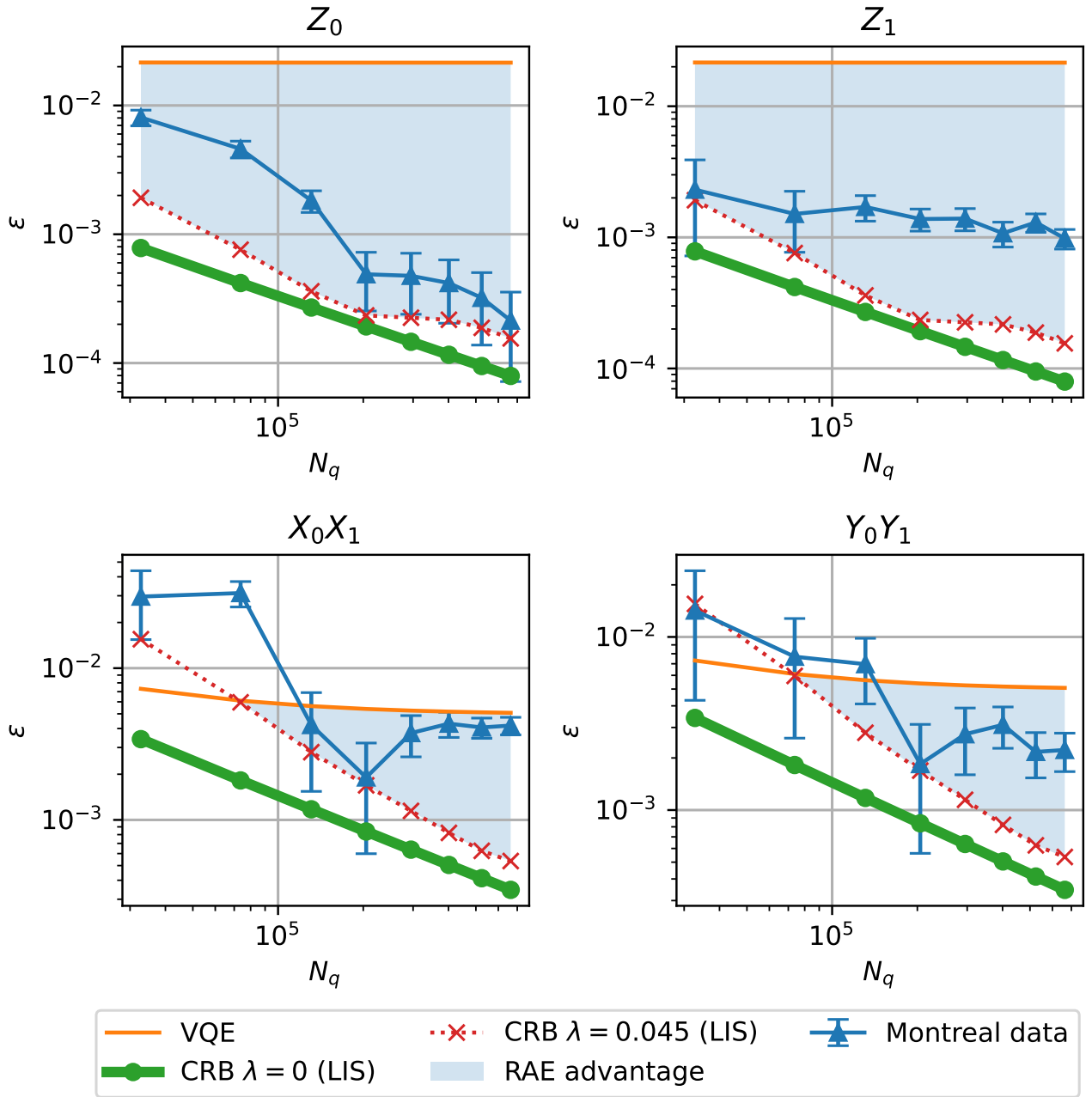


FIG. 6. RMSE of the estimated Pauli terms in the two-qubit Hamiltonian (Eq. 3). N_q refers to the total number of ansatz queries across all RAE circuits to obtain a Pauli term expectation. RMSE of the direct sampling estimator (marked VQE in the figure) was modeled based on the effective noise parameter from the fitted Chebyshev likelihood functions. CRB refers to the lower estimate of RMSE based on the Cramer-Rao bound (Eq. 6)

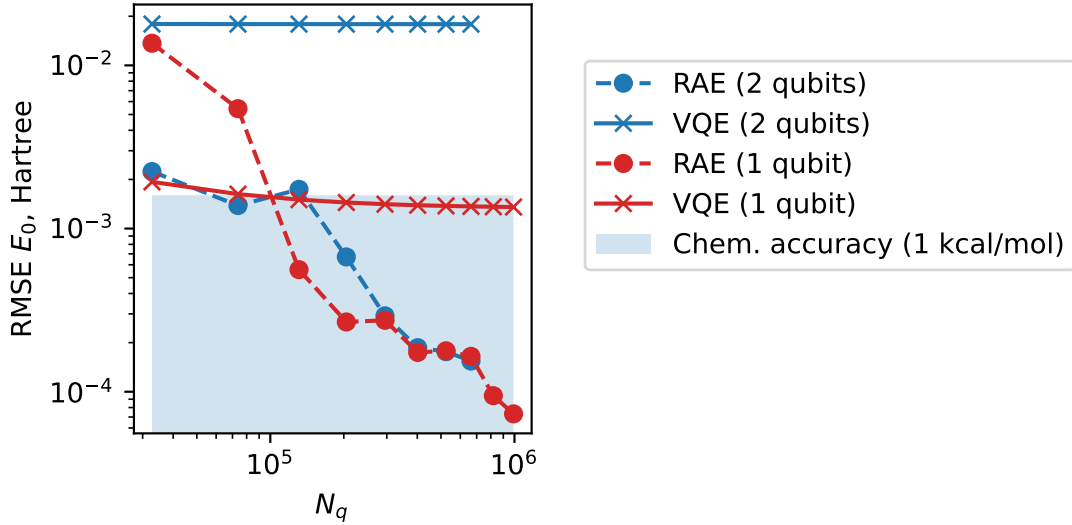


FIG. 7. Ground state energy RMSE for the one- the two-qubit Hamiltonians (Eq. 1 and Eq. 3). N_q refers to the total number of ansatz queries across all RAE circuits to obtain a Pauli term expectation assuming uniform measurement allocation. RMSE of the direct sampling estimator (marked VQE in the figure) was modeled based on the effective noise parameter (s) from the MLE and the fitted Chebyshev likelihood functions for the one- and two-qubit problems, respectively.

vergence pattern, reaching chemical accuracy at $L_{max} = 2$. In this case, RAE was superior to direct sampling across the range of N_q and improved the RMSE by about two orders of magnitude, as shown in Fig. 7. Increasing the number of ansatz queries does not result in a noticeable improvement in the energy error for the direct sampling due to the large bias. In contrast, RAE can mitigate the effect of the device noise more efficiently as more samples are included in post-processing, improving the energy RMSE by two orders of magnitude.

IV. CONCLUSIONS

This paper presented the first application of RAE to estimating the ground state energy of chemical Hamiltonians describing the hydrogen molecule in the minimum basis. RAE offers an efficient alternative to direct observable estimation, commonly used in VQE, significantly reducing the error of estimated expectation values despite relying on a simple depolarizing noise model that does not capture the complexity of decoherence effects

in realistic quantum devices. Additionally, RAE offers a more efficient way to benchmark device quality than straightforward VQE, albeit with the caveat that the underlying noise model may bias the benchmark toward certain device architectures. While the extracted noise parameter is not always a reliable indicator of device noise and can be imprecise, the convergence of the energy and its standard deviation with increasing RAE circuit layers provides an indicator of device quality without the need to compute reference data.

In contrast to previous RAE experiments that used randomized compiling to mitigate coherent error [17], we took a simpler approach by analyzing the likelihood functions for a series of IBM devices. We selected the QPU whose noise model was overall consistent with the depolarizing noise assumption, allowing us to study the impact of other factors, such as device parameter instability, on RAE performance. In particular, *ibmq_montreal* was found to exhibit both the lowest coherent error and the most stable (reproducible) effective noise parameter and was used for subsequent RAE experiments.

For the one-qubit version of the ground state energy estimation problem, the effective noise parameter was in the interval of $2 \cdot 10^{-3} - 3 \cdot 10^{-3}$ on *ibmq_montreal*. Despite low noise levels, RAE performance did not always improve as L_{max} increased, indicating the sensitivity of the method to the coherent error and discrepancies between ideal and realistic noise description. Nevertheless, the fast convergence of the total energy RMSE obtained from experimental data offered preliminary evidence of RAE advantage as an estimation technique.

In the two-qubit implementation of the ground state energy estimation, we were more limited in circuit depth due to increased noise levels, with the effective noise parameter estimated to be approximately 0.045 – 0.05. Similar to the one-qubit case, we observed fast convergence of the total energy RMSE with RAE, resulting in the error reduction from 30 mHa (in direct sampling) to approximately 0.1 mHa (best RAE estimate).

In both experiments, RAE performed better for the expectation values of the Pauli terms, which exhibited large biases in direct sampling, resulting in effective error reduction. In view of this noise mitigation property, an important direction of future work is to compare the results of RAE to those of error-mitigated VQE under a fixed shot budget. Error mitigation techniques such as zero-noise extrapolation [39–41], probabilistic error cancellation [39, 40], and Clifford data regression [42, 43] can reduce the bias of estimated expectation values in hardware experiments at the expense of allocating addi-

tional samples to infer the relevant aspects of device noise. Under a fixed measurement budget, however, this may increase sampling noise (i.e., the standard deviation of the estimator). The problem is further aggravated when several techniques are combined in an error mitigation pipeline [44]. In contrast, RAE can optimize quantum resource usage by tuning the layer schedule and shot allocation subject to constraints, yielding an overall improvement of RMSE [14].

A major limitation of the near-term RAE is its incompatibility with grouping techniques, precluding faithful comparisons to the most advanced observable estimation routines applied in VQE. Fault-tolerant computation protocols can overcome this restriction. In particular, advances in Hamiltonian encoding [45–48] could unlock new applications of RAE in the emerging era of early fault-tolerant quantum computing [49]. Exploring corresponding algorithmic trade-offs is an important direction of future research, paving the way to further enhancing the utility of RAE in quantum chemistry.

ACKNOWLEDGEMENTS

The authors acknowledge insightful discussions and suggestions from Maxwell Radin, Peter Johnson, Yanbing Zhou, and Amara Katarbarwa. Numerical results were generated using the Orquestra® platform by Zapata Computing, Inc.

Appendix A: Noisy Chebyshev likelihood functions

Chebyshev likelihood functions fitted to experimental data for *ibmq_hanoi*, *ibmq_sydney*, *ibmq_toronto*, and *ibmq_montreal* are presented in Fig. A1. Noise parameters corresponding to the solid lines can be found in Tab. A1 along with the error bars.

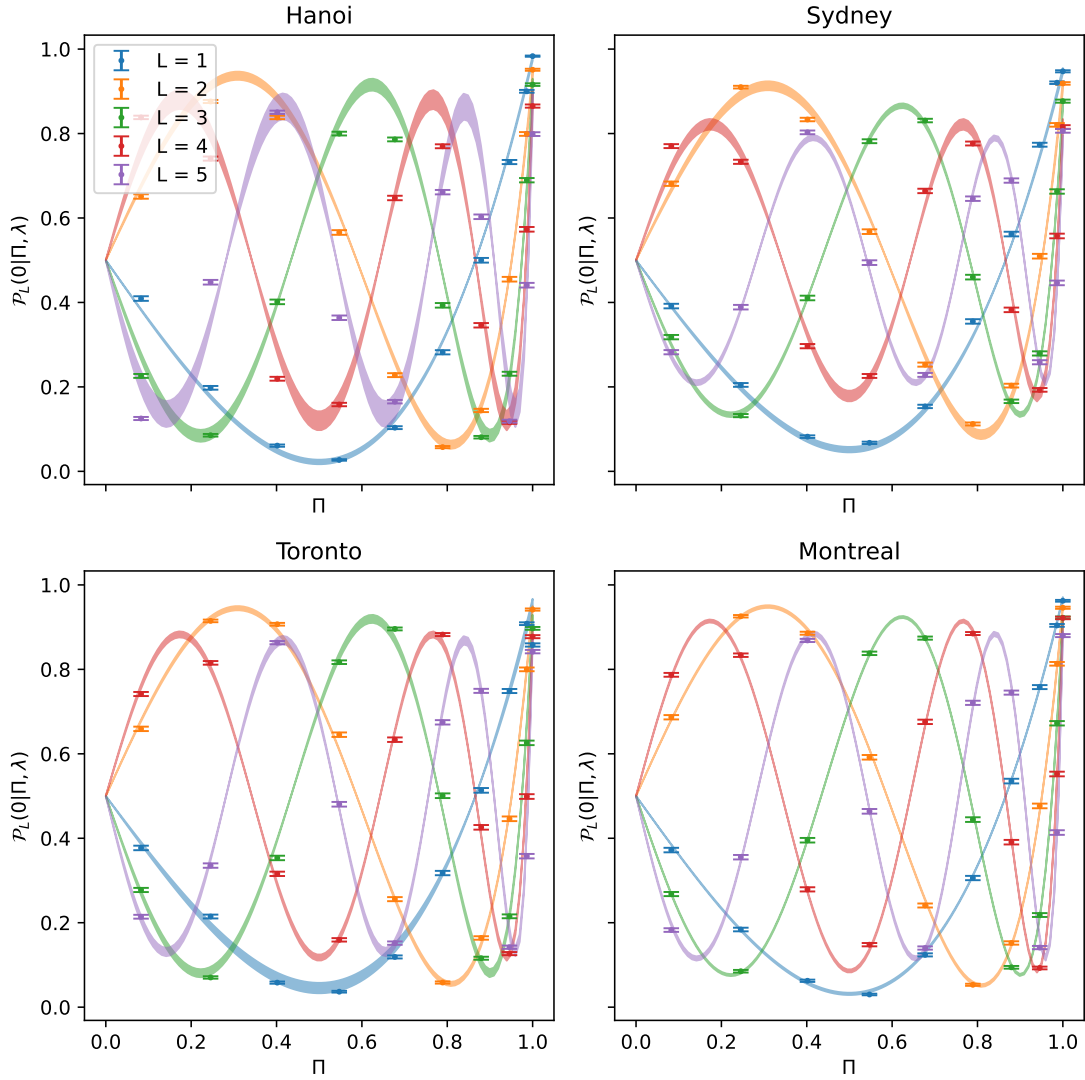


FIG. A1. The likelihood of obtaining even bitstrings when measuring X_0X_1 for RAE circuits with $L = 1, 2, 3, 4, 5$ on premium IBM devices. Solid lines represent least squares fits to experimentally estimated likelihood values.

backend/L	1	2	3	4	5
Hanoi	0.030(7)	0.054(9)	0.053(10)	0.061(13)	0.058(15)
Montreal	0.043(4)	0.043(3)	0.047(2)	0.042(2)	0.048(2)
Sydney	0.072(9)	0.076(10)	0.089(4)	0.098(9)	0.099(4)
Toronto	0.063(18)	0.047(4)	0.050(6)	0.059(4)	0.055(5)

TABLE A1. Effective noise parameters λ from fitted likelihood functions shown in Fig. A1

Appendix B: Analysis of the likelihood functions for the one-qubit RAE

To extract expectation values from the RAE experiment data, we computed the log-likelihood functions $l(\mathbf{d}; \Pi)$ for X_0 and Y_0 terms in the one-qubit molecular Hamiltonian on the uniform grids having 100 and 10000 points along λ and Π axes, respectively. As a part of the analysis, we identified the optimal inference intervals for λ and Π that were later used to obtain numerical estimates of the expectation values.

Unique maxima were identified for all the likelihood functions. In Fig. B2, we show a representative plot of $l(\mathbf{d}; \Pi)$ for X_0 on *ibmq_montreal*. As the maximum number of RAE layers increased from 1 to 10, the bootstrap MLE estimates (red crosses in Fig. B2) of $\langle X_0 \rangle$ approached the exact expectation value (marked with the vertical dashed line). The appearance of the log-likelihood functions for $L = 0$ and $L \neq 0$ is qualitatively different. As expected from Eq. 10, maximum likelihood estimates of the Pauli expectations for the former are not well defined, i.e., the likelihood functions have degenerate maxima, making it impossible to identify a unique (Π, λ) pair as shown in Fig. B3.

For this reason, λ needs to be eliminated from MLE to obtain unique estimates of Pauli expectations for $L = 0$. To this end, we set it to 0 when extracting the expectation values. It can be shown that such approach is equivalent to the direct sampling used in standard VQE⁸. The ground state energies estimated from the individual Pauli expectations with this method are reported in Table B2.

The ground state energies are close to the noiseless reference, consistent with generally low noise levels in one-qubit experiments, except for *ibmq_toronto*.

⁸ Indeed, the log-likelihood function in this case is $l(\mathbf{d}; \Pi) \propto \log(1 - \Pi)(N_s - e_0) + \log(1 + \Pi)e_0$, and the MLE estimate of Π is $\hat{\Pi} = \frac{2e_0 - N_s}{N_s}$

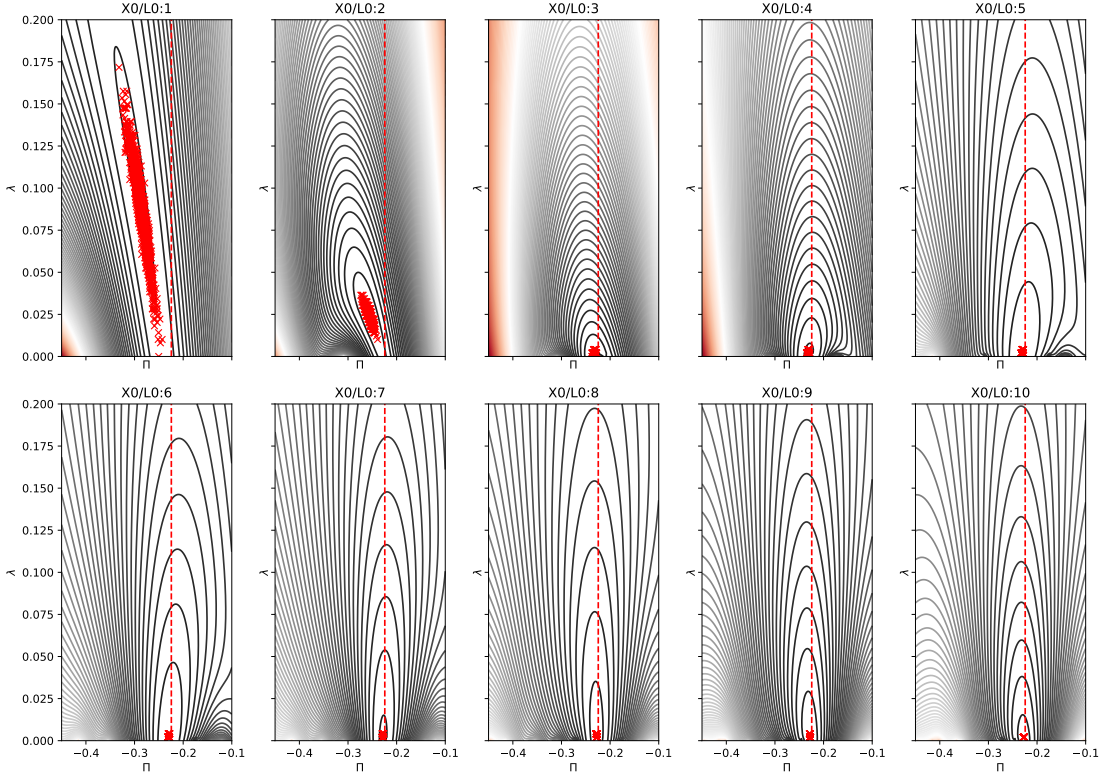


FIG. B2. Log-likelihood functions for X_0 generated from RAE experimental data on *ibmq_montreal*. The vertical dashed line shows the reference expectation value. Red crosses mark the MLE from 1000 bootstrap runs. L0:X notation indicates that we included samples from RAE circuits with 0, 1, ..., X layers when calculating the likelihood function. Darker colors correspond to larger values of $l(\mathbf{d}; \Pi)$.

backend	Hanoi	Sydney	Toronto	Montreal
E, Ha	-1.1373(27)	-1.1370(24)	-1.0451(51)	-1.1348(32)
RMSE, mHa	3	3	92	4

TABLE B2. Ground state energy estimates and their RMSE for the one-qubit problem calculated via MLE with $\lambda = 0$ (i.e., standard sampling) and 25000 bootstrap samples

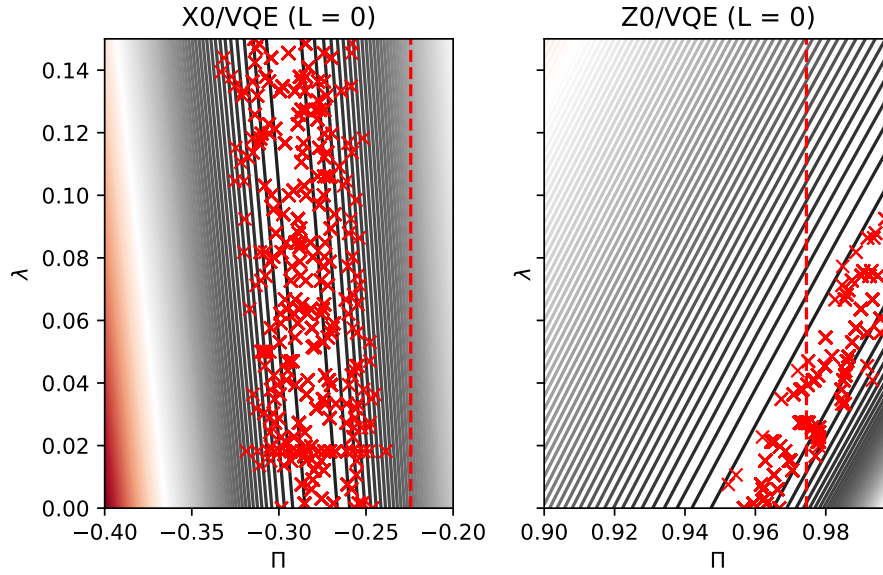


FIG. B3. Log-likelihood functions for X_0 , Z_0 generated from the RAE experiment data on *ibmq_montreal* for $L = 0$. Vertical dashed lines mark exact (noiseless) values. Red crosses represent the MLE from 5000 bootstrap runs. Darker colors correspond to larger values of the log-likelihood.

Appendix C: Analysis of the likelihood functions for the two-qubit RAE

Compared to the one-qubit problem, the two-qubit expectation value estimation is more challenging due to the faster accumulation of coherent error with increased Grover depth. When analyzing the results of the two-qubit RAE experiments, we identified different convergence patterns exemplified in Fig. C4 for *ibmq_montreal*. Although all the estimates tend to stabilize as the maximum number of layers is increased from 1 to 8, some may have sizable fluctuations deviating from the exact value as L_{max} approaches 8. Likewise, the maximum of the log-likelihood shifts along the λ axis as L_{max} increases for Z_0 , which can be related to device parameter instability.

As explained in Appendix B, MLE cannot be directly applied to the set of samples for $L = 0$ unless the nuisance parameter λ is eliminated from the inference. Using this

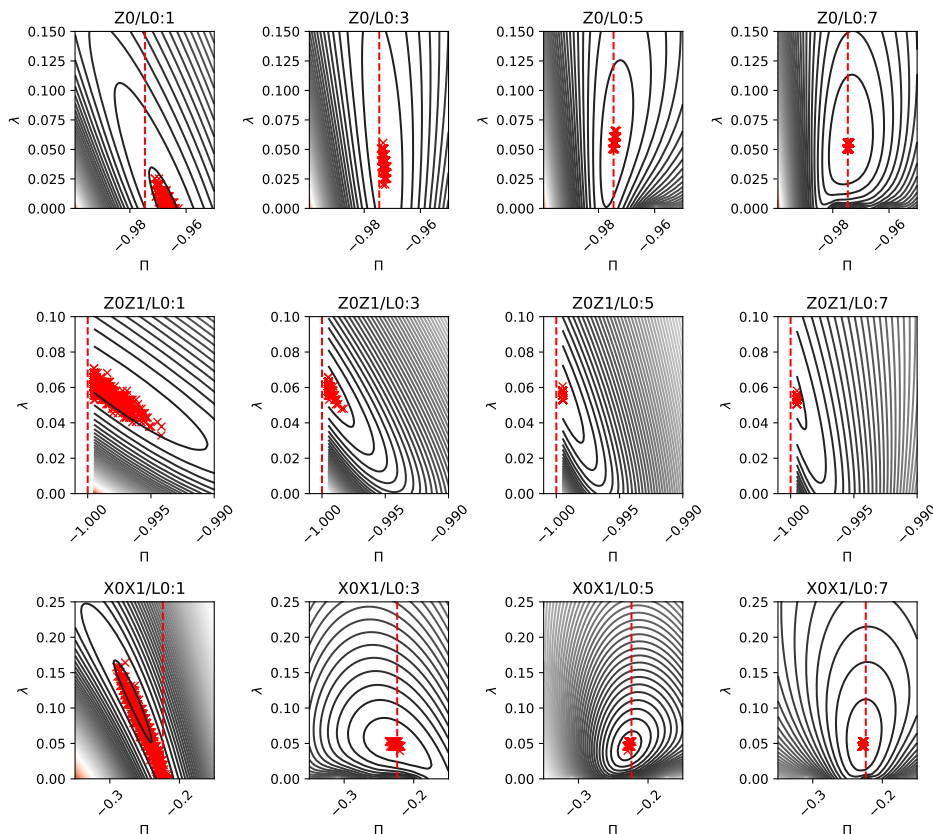


FIG. C4. Log-likelihood functions for Z_0 , Z_0Z_1 and X_0X_1 on *ibmq_montreal*. Vertical dashed lines mark exact (noiseless) expectation values. Red crosses represent the MLE from 1000 bootstrap samples. Darker lines correspond to larger values of the log-likelihood.

backend	Hanoi	Sydney	Toronto	Montreal
E, Ha	-1.1047(29)	-1.0889(31)	-1.1156(26)	-1.11282(29)
RMSE, mHa	41	57	30	33

TABLE C3. Reference VQE energies and their RMSE for the 2-qubit ground state energy estimation problem

approach, we obtained the estimates of the ground state energy, reported in Tab. C3

Appendix D: Noise Robust Incremental Sequence

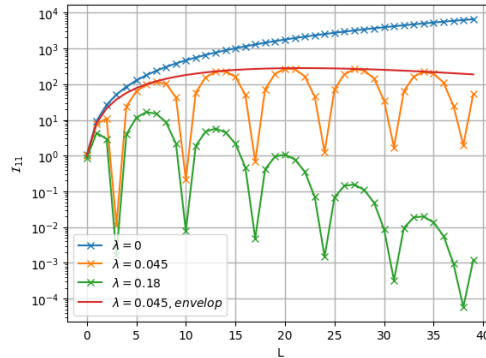


FIG. D5. Fisher information of X_0X_1 where $\langle X_0X_1 \rangle \approx -0.2237$ versus number of Grover layers L , under effective noise parameter $\lambda = 0, 0.045, 0.18$.

In this Appendix, we discuss the method we used to optimize incremental sequence in the presence of noise. It can be viewed as an adaptation of the approach presented by Giurgica-Tiron et al. [14] to the problem of optimal shot allocation based on maximizing noisy Fisher information. Specifically, we explored a setting where the number of shots per RAE circuit is kept fixed while the Grover depth is subject to optimization. As one can see in Fig. D5, while the Fisher information grows with the number of Grover layers in the absence of decoherence effects, i.e., $\lambda = 0$, it behaves differently when effective noise $\lambda > 0$. The latter features an oscillation pattern with a period of approximately 7. It is desirable to design a layer schedule such that the local minima of Fisher information are avoided. This is achieved for the values of L satisfying an approximate condition:

$$\sin^2((2L + 1) \operatorname{acos}(\Pi)) \approx 1, L \in \mathbb{Z}. \quad (\text{D1})$$

For the edge case where $\Pi \approx \pm 1$, the above condition is hard to satisfy, and the exponential incremental sequence is optimal, which coincides with the noiseless situation.

The oscillation has an envelope with a maximum at a certain number of Grover layers for noisy situations, whose analytical form can be derived by substituting condition D1 to the Fisher information (Eq. 14):

$$\mathcal{I}(\Pi, \lambda)_{11, \text{envelop}} = \frac{(2L + 1)^2 e^{-\lambda(2L+1)}}{(1 - \Pi^2)}. \quad (\text{D2})$$

The number of Grover layers $L_{\max \mathcal{I}}$ that maximizes $\mathcal{I}(\Pi, \lambda)_{11, \text{envelop}}$ is the only root of equation $\frac{\partial \mathcal{I}(\Pi, \lambda)_{11, \text{envelop}}}{\partial L} = 0$, which yields $L_{\max \mathcal{I}} = \frac{1}{\lambda} + \frac{1}{2}$. This result is consistent with Fig. D5 where Fisher information reaches maxima at $L_{\max \mathcal{I}} \approx 22$ and 5 for $\lambda = 0.045$ and 0.18, respectively.

Based on the discussion above, we designed our noise robust incremental sequence as follows:

- Measure λ and calculate $L_{\max \mathcal{I}}$; choose a hyperparameter $c > 0$
- If $|\Pi| < c\lambda$ or $1 - |\Pi| < c\lambda$, do exponential incremental sequence.
- Otherwise, the incremental sequence is constructed by L that satisfy:
 - $\sin^2((2L + 1) \operatorname{acos}(\Pi)) > 1 - c\lambda$
 - $L \in \mathbb{Z}$
 - $L < L_{\max \mathcal{I}}$

We compared the performance of different incremental sequences in Fig. D6. Our noise-robust incremental sequence reaches minimum error with fewer queries than linear and exponential ones. However, the minimum error reached is larger compared to the other two sequences. This could be due to our model assumptions regarding device noise that ignore the complexity of decoherence effects on real hardware.

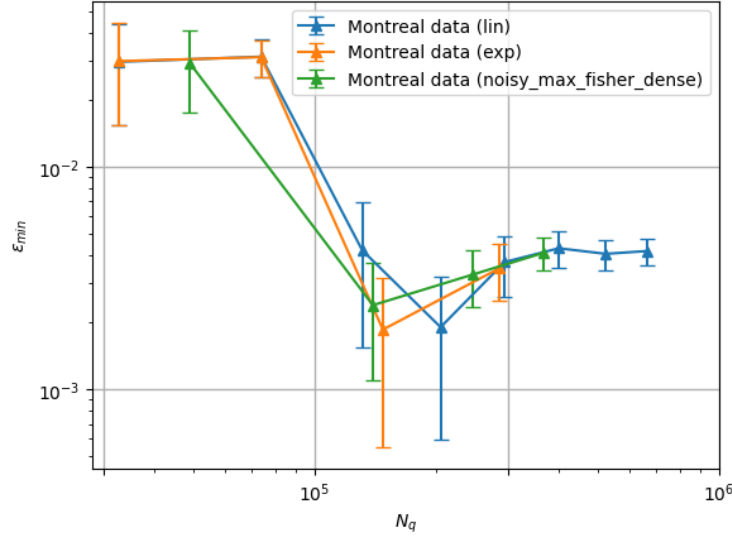


FIG. D6. The comparison between incremental sequences (Linear, Exponential, and Noise robust) for Montreal data.

-
- [1] A. M. Dalzell, S. McArdle, M. Berta, P. Bienias, C.-F. Chen, A. Gilyén, C. T. Hann, M. J. Kastoryano, E. T. Khabiboulline, A. Kubica, G. Salton, S. Wang, and F. G. S. L. Brandão, Quantum algorithms: A survey of applications and end-to-end complexities (2023), arXiv:2310.03011 [quant-ph].
 - [2] G. Wang, D. E. Koh, P. D. Johnson, and Y. Cao, Minimizing estimation runtime on noisy quantum computers, PRX Quantum **2**, 010346 (2021).
 - [3] D. E. Koh, G. Wang, P. D. Johnson, and Y. Cao, A framework for engineering quantum likelihood functions for expectation estimation, arXiv:2006.09349v1.
 - [4] Y. Suzuki, S. Uno, R. Raymond, T. Tanaka, T. Onodera, and N. Yamamoto, Amplitude estimation without phase estimation, Quantum Information Processing **19**, 75 (2020), arXiv:1904.10246 [quant-ph].
 - [5] T. Tanaka, Y. Suzuki, S. Uno, R. Raymond, T. Onodera, and N. Yamamoto, Amplitude estimation via maximum likelihood on noisy quantum computer, Quantum Information Processing **20**, 293 (2021).
 - [6] J. F. Gonthier, M. D. Radin, C. Buda, E. J. Duskocil, C. M. Abuan, and J. Romero, Measurements as a roadblock to near-term practical quantum advantage in chemistry: Resource anal-

- ysis, *Physical Review Research* **4**, 033154 (2022).
- [7] A. Peruzzo, J. McClean, P. Shadbolt, M.-H. Yung, X.-Q. Zhou, P. J. Love, A. Aspuru-Guzik, and J. L. O'Brien, A variational eigenvalue solver on a photonic quantum processor, *Nat. Commun.* **5**, 4213 (2014).
- [8] P. D. Johnson, A. A. Kunitsa, J. F. Gonthier, M. D. Radin, C. Buda, E. J. Doskocil, C. M. Abuan, and J. Romero, Reducing the cost of energy estimation in the variational quantum eigensolver algorithm with robust amplitude estimation (2022).
- [9] L. B. Otfelie, M. Urbanek, M. Metcalf, J. Carter, A. F. Kemper, and W. A. d. Jong, Simulating quantum materials with digital quantum computers, *Quantum Science and Technology* **6**, 043002 (2021).
- [10] D. Jaksch, P. Givi, A. J. Daley, and T. Rung, Variational Quantum Algorithms for Computational Fluid Dynamics (2022), arXiv:2209.04915 [physics, physics:quant-ph].
- [11] F. Y. Leong, W.-B. Ewe, and D. E. Koh, Variational Quantum Evolution Equation Solver, *Scientific Reports* **12**, 10817 (2022), arXiv:2204.02912 [physics, physics:quant-ph].
- [12] R. Hayakawa, Quantum algorithm for persistent Betti numbers and topological data analysis, *Quantum* **6**, 873 (2022).
- [13] D. W. Berry, Y. Su, C. Gyurik, R. King, J. Basso, A. D. T. Barba, A. Rajput, N. Wiebe, V. Dunjko, and R. Babbush, Analyzing Prospects for Quantum Advantage in Topological Data Analysis, *PRX Quantum* **5**, 010319 (2024).
- [14] T. Giurgica-Tiron, I. Kerenidis, F. Labib, A. Prakash, and W. Zeng, Low depth algorithms for quantum amplitude estimation, *Quantum* **6**, 745 (2022), arXiv:2012.03348 [quant-ph].
- [15] T. Giurgica-Tiron, S. Johri, I. Kerenidis, J. Nguyen, N. Plesch, A. Prakash, K. Sosnova, K. Wright, and W. Zeng, Low-depth amplitude estimation on a trapped-ion quantum computer, *Physical Review Research* **4**, 033034 (2022).
- [16] A. Katabarwa, A. Kunitsa, B. Peropadre, and P. Johnson, Reducing runtime and error in VQE using deeper and noisier quantum circuits (2021), arXiv:2110.10664 [quant-ph].
- [17] A. Dalal and A. Katabarwa, Noise tailoring for robust amplitude estimation, *New Journal of Physics* **25**, 023015 (2023).
- [18] D. Grinko, J. Gacon, C. Zoufal, and S. Woerner, Iterative Quantum Amplitude Estimation, *npj Quantum Information* **7**, 52 (2021), arXiv:1912.05559 [quant-ph].
- [19] P. Rao, K. Yu, H. Lim, D. Jin, and D. Choi, Quantum amplitude estimation algorithms on ibm

- quantum devices, in *Quantum Communications and Quantum Imaging XVIII*, Vol. 11507 (SPIE, 2020) pp. 49–60.
- [20] S. Simon, M. Degroote, N. Moll, R. Santagati, M. Streif, and N. Wiebe, Amplified amplitude estimation: Exploiting prior knowledge to improve estimates of expectation values, arXiv preprint arXiv:2402.14791 (2024).
- [21] S. Dasgupta and T. S. Humble, Stability of noisy quantum computing devices, arXiv preprint arXiv:2105.09472, 1 (2021), arXiv:2105.09472.
- [22] T. Tanaka, S. Uno, T. Onodera, N. Yamamoto, and Y. Suzuki, Noisy quantum amplitude estimation without noise estimation, *Physical Review A* **105**, 012411 (2022), arXiv:2110.04258 [quant-ph].
- [23] C. Hempel, C. Maier, J. Romero, J. McClean, T. Monz, H. Shen, P. Jurcevic, B. P. Lanyon, P. Love, R. Babbush, A. Aspuru-Guzik, R. Blatt, and C. F. Roos, Quantum Chemistry Calculations on a Trapped-Ion Quantum Simulator, *Physical Review X* **8**, 031022 (2018).
- [24] J. Romero, R. Babbush, J. R. McClean, C. Hempel, P. Love, and A. Aspuru-Guzik, Strategies for quantum computing molecular energies using the unitary coupled cluster ansatz (2018), arXiv:1701.02691 [quant-ph].
- [25] A. Zhao, A. Tranter, W. M. Kirby, S. F. Ung, A. Miyake, and P. J. Love, Measurement reduction in variational quantum algorithms, *Physical Review A* **101**, 062322 (2020).
- [26] V. Verteletskyi, T.-C. Yen, and A. F. Izmaylov, Measurement optimization in the variational quantum eigensolver using a minimum clique cover, arXiv:1907.03358v4.
- [27] P. Gokhale, O. Angiuli, Y. Ding, K. Gui, T. Tomesh, M. Suchara, M. Martonosi, and F. T. Chong, Minimizing State Preparations in Variational Quantum Eigensolver by Partitioning into Commuting Families (2019), arXiv:1907.13623.
- [28] T.-C. Yen and A. F. Izmaylov, Cartan subalgebra approach to efficient measurements of quantum observables, *PRX quantum* **2**, 040320 (2021).
- [29] A. F. Izmaylov, T.-C. Yen, R. A. Lang, and V. Verteletskyi, Unitary partitioning approach to the measurement problem in the Variational Quantum Eigensolver method (2019).
- [30] L. Wasserman, *All of Statistics: A Concise Course in Statistical Inference*, Springer Texts in Statistics (Springer, New York, NY, 2004).
- [31] E. G. Brown, O. Goktas, and W. K. Tham, Quantum Amplitude Estimation in the Presence of Noise (2020), arXiv:2006.14145 [quant-ph].

- [32] A. Callison and D. E. Browne, Improved maximum-likelihood quantum amplitude estimation (2023), arXiv:2209.03321 [quant-ph].
- [33] A. W. Cross, L. S. Bishop, S. Sheldon, P. D. Nation, and J. M. Gambetta, Validating quantum computers using randomized model circuits, *Physical Review A* **100**, 032328 (2019), publisher: American Physical Society.
- [34] R. Blume-Kohout and K. C. Young, A volumetric framework for quantum computer benchmarks, *Quantum* **4**, 362 (2020), publisher: Verein zur Förderung des Open Access Publizierens in den Quantenwissenschaften.
- [35] S. Bravyi, S. Sheldon, A. Kandala, D. C. McKay, and J. M. Gambetta, Mitigating measurement errors in multi-qubit experiments, *Physical Review A* **103**, 10.1103/PhysRevA.103.042605 (2021).
- [36] P. Virtanen, R. Gommers, T. E. Oliphant, M. Haberland, T. Reddy, D. Cournapeau, E. Burovski, P. Peterson, W. Weckesser, J. Bright, S. J. van der Walt, M. Brett, J. Wilson, K. J. Millman, N. Mayorov, A. R. J. Nelson, E. Jones, R. Kern, E. Larson, C. J. Carey, Í. Polat, Y. Feng, E. W. Moore, J. VanderPlas, D. Laxalde, J. Perktold, R. Cimrman, I. Henriksen, E. A. Quintero, C. R. Harris, A. M. Archibald, A. H. Ribeiro, F. Pedregosa, P. van Mulbregt, and SciPy 1.0 Contributors, SciPy 1.0: Fundamental Algorithms for Scientific Computing in Python, *Nature Methods* **17**, 261 (2020).
- [37] B. Efron and R. J. Tibshirani, *An Introduction to the Bootstrap* (Chapman and Hall/CRC, New York, 1994).
- [38] A. Javadi-Abhari, M. Treinish, K. Krsulich, C. J. Wood, J. Lishman, J. Gacon, S. Martiel, P. D. Nation, L. S. Bishop, A. W. Cross, B. R. Johnson, and J. M. Gambetta, Quantum computing with Qiskit (2024), arXiv:2405.08810 [quant-ph].
- [39] K. Temme, S. Bravyi, and J. M. Gambetta, Error Mitigation for Short-Depth Quantum Circuits, *Physical Review Letters* **119**, 180509 (2017), publisher: American Physical Society.
- [40] A. Kandala, K. Temme, A. D. Córcoles, A. Mezzacapo, J. M. Chow, and J. M. Gambetta, Error mitigation extends the computational reach of a noisy quantum processor, *Nature* **567**, 491 (2019), publisher: Nature Publishing Group.
- [41] M. Krebsbach, B. Trauzettel, and A. Calzona, Optimization of Richardson extrapolation for quantum error mitigation, *Physical Review A* **106**, 062436 (2022), arXiv:2201.08080 [cond-mat, physics:quant-ph].

- [42] P. Czarnik, A. Arrasmith, P. J. Coles, and L. Cincio, Error mitigation with Clifford quantum-circuit data, *Quantum* **5**, 592 (2021), arXiv:2005.10189 [quant-ph].
- [43] A. Lowe, M. H. Gordon, P. Czarnik, A. Arrasmith, P. J. Coles, and L. Cincio, Unified approach to data-driven quantum error mitigation, *Physical Review Research* **3**, 033098 (2021), arXiv:2011.01157 [quant-ph].
- [44] A. A. Saki, A. Katarbarwa, S. Resch, and G. Umbrurescu, Hypothesis Testing for Error Mitigation: How to Evaluate Error Mitigation (2023), arXiv:2301.02690 [quant-ph].
- [45] I. Loaiza, A. M. Khah, N. Wiebe, and A. F. Izmaylov, Reducing molecular electronic Hamiltonian simulation cost for linear combination of unitaries approaches, *Quantum Science and Technology* **8**, 035019 (2023).
- [46] I. Loaiza and A. F. Izmaylov, Block-Invariant Symmetry Shift: Preprocessing Technique for Second-Quantized Hamiltonians to Improve Their Decompositions to Linear Combination of Unitaries, *Journal of Chemical Theory and Computation* **19**, 8201 (2023).
- [47] I. Loaiza and A. F. Izmaylov, Majorana Tensor Decomposition: A unifying framework for decompositions of fermionic Hamiltonians to Linear Combination of Unitaries (2024), arXiv:2407.06571 [physics, physics:quant-ph].
- [48] D. Rocca, C. L. Cortes, J. F. Gonthier, P. J. Ollitrault, R. M. Parrish, G.-L. Anselmetti, M. Degroote, N. Moll, R. Santagati, and M. Streif, Reducing the Runtime of Fault-Tolerant Quantum Simulations in Chemistry through Symmetry-Compressed Double Factorization, *Journal of Chemical Theory and Computation* **20**, 4639 (2024).
- [49] A. Katarbarwa, K. Gratsea, A. Caesura, and P. D. Johnson, Early Fault-Tolerant Quantum Computing, *PRX Quantum* **5**, 020101 (2024).